Computational and Theoretical Chemistry 1217 (2022) 113929

Contents lists available at ScienceDirect

Computational and Theoretical Chemistry

journal homepage: www.elsevier.com/locate/comptc

Comparative analyses and molecular videography of MD simulations on WT human SOD1

Aron S. Workman

AXOXY Laboratories LLC, Weston, FL 33326, USA

ARTICLE INFO

Keywords:
Superoxide dismutase 1 (SOD1)
Crystallographic template
Reference structure constructs
Fragmented active site (FAS)
Molecular dynamics (MD)
Molecular graphics and videography

ABSTRACT

Cu/Zn superoxide dismutase (SOD1) is the antioxidant enzyme that catalyses intracellular superoxide radical. In this study, the molecular dynamics (MD) of six wild-type (WT) human (h) SOD1 PDB crystallographs were computed to comparative analyses and visualisations, including a novel method of high-resolution molecular videography. Production MD were computed across variable matrix conditions for 10 ns (0.01 ns resolution), 37 °C and pH 7.4. MD simulations yielded PCA, RMSD, RMSF, SAS, S—S bonds, and H bonds analyses. The attached molecular video comprises 20 s of MD footage at 540p/48 Hz resolution featuring 10 ns of computed trajectories. Of PDB IDs 1HL5, 1PU0, 1SPD, 2C9V, and 2V0A, this study determines that 1PU0 should be implemented as the ideal crystallographic template for ongoing computational works on hSOD1.

1. Introduction

Wild-type (WT) human (h) Cu/Zn superoxide dismutase (SOD1) is a widely-studied metalloprotein, yet the literature is hitherto without a critical comparative analysis of its crystallographs. Comparative analyses of protein crystallographs enable rational selection of a reference structure for use as a template in the computational study of its biochemistry. The comparative analyses of this work identify the strengths and weaknesses of WT hSOD1 crystallographs, which is of concern for selection strategy in experimental design. Precedent is also hitherto absent a generalizable method for high-resolution molecular videography. Molecular videographs are rare, and there are hitherto no known molecular videographs of SOD1. The molecular videography of this work are comprised of frame animations of sequential computational results of MD computations. The resultant cinematic sequences of WT hSOD1 are given in high-resolution video. Methods including scripts are given for the high-resolution molecular videography methodology, which can be generalized for videographic usage of other dynamic proteins by trivial customization.

WT hSOD1 is the vital metalloenzymatic antioxidant that controls the counter-proliferation of volatile superoxide radicals via an ultra-fast catalysed dissipation from matrix. WT SOD1 is relevant to myriad fundamental biochemical pathways and processes including aerobic metabolism, cell cycling, and biological signaling. WT hSOD1 is a complex metalloenzyme that binds a copper ion, a zinc ion, and an intra-disulfide bond per each of two subunits, comprising its native homodimer. SOD1 maturation are the complex time-dependent post-translational interactions and reactions that serve to activate the enzymic function of SOD1 through the concomitant installation events of metallation, dimerisation, and intra-disulfide bonding.

Functional SOD1 holoenzyme is the most critical evolutionary adaptation of the last two billion years. A revolution in oxygenic photosynthesis flooded the Paleoproterozoic atmosphere with free oxygen, which caused an attenuation of work and concomitant mass extinction event [1]. The developments of multicellularity, photosynthesis, and aerobic metabolism were endangered as life on Earth first realized the hostile reality of oxygenated air. Aerobes are still extant due to the latent and punctate emergence of SOD1, which became the primary molecular counteragent reacting to quench radicalized free oxygen [2]. The molecular evolution of SOD1 enabled the sustained evolution of aerobic organisms [3].

Molecular dynamics (MD) is a computational biochemistry methodology that solves the time-dependent coordinates of a biomolecule in parameterized aqueous matrix [4]. MD computations are predominantly iterative calculations of Newtonian equations of motion which yield the resultant atomistic trajectories. MD simulations are commonly used to observe the time-dependency of coarse biomolecular phenomena and gross biomolecular behavior such as protein folding, multimerisation, ligand binding, and non-covalent interaction. MD simulation durations are constrained by theoretical limits and current supercomputing workflows to about one microsecond. Protein-ligand interaction studies utilizing MD simulations dominate the discovery and development of

E-mail address: aron@axoxy.com.

https://doi.org/10.1016/j.comptc.2022.113929
Received 8 June 2022; Received in revised form 25 October 2022; Accepted 26 October 2022
Available online 31 October 2022

ligand effectors as an oft-traversed annal of pharmaceutics [5]. High-resolution time-dependency of fine biomolecular motions, switches, thresholds, and events such as ultra-fast decompositions, transition state formations, and ionic and covalent bindings are also increasingly achievable. The time-dependent datasets obtained via simulation do not commonly have a correlate or even comparable experimental result capable of being drawn from the wet biophysics lab [6]. Even in the absence of comparable data *in vitro*, specific modes of analysis *in silico* steer critical validators, parameters, and controls over the factors and functions which likely contribute to its theoretical accuracy.

Classical simulations can be initialized from fine structure obtained from quantum mechanics (QM) computations [7,8]: QM computations were prepared to yield the coordinates for key SOD1 conformations of free and bound transition states and reaction intermediates having proximity to the SOD1 active site [9]. Fragmented active site (FAS) QM/MD is a hybrid QM/MM method derived from fragment models and closely related to FMO-MD. FAS QM/MD was used to determine the starting structures, molecular parameters, and iterative minimizations of metallic and inorganic ions, metallic and sulfidic cofactors, molecular fragments of clusters and residues, and substrate and product. FAS QM/MD coordinates preceded and were computed independent from the MD workflow [10,11].

Recent MD simulations for SOD1 which also report methodological advancements include discrete molecular dynamics with FMO calculations [12–14], steered molecular dynamics with geometric sampling [15,16], coarse-grained molecular dynamics [17], artificial intelligence (neural network) acceleration [18], custom CHARMM parameterizations [19], and basic metadynamics [20]. Myriad MD studies both on SOD1 and other computational constructs contributed as precedent [13,21–36,36–50].

The simulations of this manuscript are high-resolution rather than extended-time in order to analyze the matrix, metadynamics, and mechanics. In the case of WT hSOD1, a short simulation duration of just 10 ns eludes just dimerization and folding – intradisulfide bonding, metallic bonding, salt bridging, and substrate reactions and interactions are observed over the order of the nanosecond and femtosecond. SOD1 is a well-studied beta-barrel that is frequently used as a template or placeholder protein in biophysical studies wherein the actual impetus of the study are the methodological or analytical advancements.

In this work, WT hSOD1 reference structure constructs were each computed to MD simulation along with myriad experimental isoforms, structural derivatives, and protein–ligand complexes. The constructs studied in this work were initially derived from X-ray crystallographs with PDB IDs 1HL5 [51], 1PU0 [52], 1SPD [53], 2C9V [54], and 2V0A [55]. Each WT hSOD1 reference structure constructs were computed and analysed to establish baselines, draw comparative conclusions, determine the ideal reference structure, and proctor novel molecular hypotheses in tests and experiments.

2. Methods

2.1. Hardware and software

Computational tasks were executed on a personal workstation comprised of a D5-powered liquid cooling path on a 1st edition AMD Ryzen Threadripper (16 cores, 32 threads) clocked at 3.4–3.8 GHz, 64 GB of quad-channel Samsung die DDR4 memory clocked at 3.0–3.3 GHz, and two x16 Nvidia GTX1080 GPUs, configured for GROMACS acceleration, clocked at 1.8–2.0 GHz (driver 415, CUDA 10). Computational data were initially processed on an M.2 SSD or 40 GB RAMDISK; static datasets were finally moved to a 4 TB SSHD for permanent reference storage. Ubuntu 18.04–18.10 was the OS used to host the software suite comprised of GROMACS, CHARMM, VMD, NWChem, PLUMED, OpenBabel, and R Statistics, python, and bash. GROningen Machine for Chemical Simulations (GROMACS) 2018.4–2019.1 was employed strictly for MD simulations [56–62] with the version 5.0 gmx sasa implementation of Van der Waals radii [63,64]; the GROMACS compilation from source with its external dependencies was challenging; the bash commands utilized to compile this GROMACS are thus given in Script S1. A custom implementation of Chemistry at HARvard Macromolecular Mechanics (CHARMM) (Nov. 2018) was freshly customized for bound metallic ions [65,66], and developed and employed as its force field [67], which was integrated with GROMACS [68,69]. Visual Molecular Dynamics (VMD) was employed strictly for visualizations [70]. Northwest Computational Chemistry Package (NWChem) was employed for the quantum mechanical (QM) chemistry models and computations [71].

2.2. QM computations

Quantum mechanical (QM) computations were executed in the gas phase. Computations implemented hybrid open-shell density functional theory (ODFT) with spherical-harmonic angular basis functions. CAM-B3LYP was selected as the gradient approximation exchange correlation *(XC)* function for a coulomb-attenuated range-adjusted correctional functional used to study electron transfers at a distance [72–75]. Pople 6-311++G** and Dunning aug-cc-pVTZ basis sets were selected as the ODFT basis sets due to their diffusion, polarization, and interoperability settings [76,77]. The basis sets were chosen for their expansive orbital models and compatibility with organic atoms and copper and zinc ion.

2.3. FAS QM/MD model

Fragmented active site (FAS) QM/MD is a hybrid QM/MM method which computes FAS fragments as extracted from the dissection of a structural model. FAS QM/MD can drastically improve the accuracy of simulations relative to comparable results of simulations without using FAS QM/MD. QM computes the molecular orbitals (MO) of subatomistic coordination chemistries, whereas MD computations construct atomic structures with atomistic coordinates. The fine structure resolutions within the QM fragments are utilized to resolve the protein–ligand interactions of bound transition states and transition metals: Cu-I, Cu-II, and Zn-II ions are found differentially bound to native SOD1. WT hSOD1 holoenzyme binds active site chemistries grossly comprised of (HisH43), HisD48, HisE46, HisE110, HisD120, HisE63, HisE80, HisE71, Asp83, Cu-II, and Zn-II. The residues were selected according to an active site hydrogen bond analysis derived from crystallographic template [78]. Each residue of the active site were each converted to fragments, and each fragment were computed both alone and of the parent hybrid. Minimum potentials were then resolved by minimizing the equation: $E = E_{QM}(QM) + E_{MD}(QM + MD) - E_{MD}(QM)$. The resultant coordinates of the reassembled hybrid are included in the early MD workflow by reconstruction of the initial structure to include the newly resolved coordinate definitions and parameterizations.

2.4. FF parameterizations

SOD1 binds Cu-II ion and Zn-II ion with probable transition states to Cu-I ion and Zn-II ion, but CHARMM36 does not include potentials for these metallic ions. Thus, semi-novel CHARMM36 force field parameterizations were prepared for Cu-II, Zn-II, and Cu-I as bound to the SOD1 active site. Custom solutions to missing CHARMM36 potentials for the MD of metalloenzyme were previously solved by similar methods. The solution potentials should be recalculated when computing a simulation of different structure.

2.5. Preparation and two-step equilibration

Molecular dynamics (MD) preparations and equilibration were executed in the liquid phase. X-ray crystallographs were obtained from RCSB [79]. Working structures were generated by programmatically stripping the PDB file of crystalline water, sulfate, sodium, and chlorine

atoms. When more than one dimer was present in the initial crystal, just one dimer of two chains were extracted per instance of computational processing. Next, the isolated dimer was placed inside a cubic box of d = 2.0, saturated with Space Point Charge 216 (spc216) water, and neutralized with 100 mM NaCl at constant 37.0 °C. Energy minimization as Steepest Descents converged to Fmax < 100 and within the machine precision, yielding the initial configuration and EM parameters. Structures were each then simulated to a comparative analysis of 2 ns or more for a two-step equilibration at both constant pressure (NVT) and then constant volume (NPT).

2.6. Production MD

Production molecular dynamics (MD) were executed in the liquid phase. The bash commands collected in Script S2 were utilized to prepare the reference structure constructs and then execute the production MD. The Particle Mesh Ewald (PME) sum was computed in reciprocal space for electrostatic interactions [80]. The full Lennard-Jones parameter combination matrix and initializing LINear Constraint Solver (LINCS) were each employed (the center of mass motion removal mode was linear) [81], with the number of constraints for LINCS set to 2,156 [82]. Intra-simulation communication occurred every 10 steps to link all bonded simulations to atoms [83].

2.7. Data handling, statistics, and graphics

Rplot_gromacs.R 1.0.0 by Francesco Carbone (UCL, 2015) was modified to visualize the GROMACS solutions in R. Script S5 is an R script for formatting equilibrations to visualization. Script S6 is an R script for formatting MD simulations to visualization.

2.8. High-resolution molecular videography

Molecular trajectories obtained from MD simulations were initially processed for cursory tests just prior to the execution of expensive computations. Script S4 calls Script S3 to programmatically iterate the loading, selection, representation, frame capture, and high-resolution rendering of each of 6,000 frames. MD trajectories were programmatically shifted 0.01 ns forward with each successive rendering. The resultant frames were 1000 × 1000px bitmaps of 3 MB/frame. Finally, with the rendering of the initial frames complete, the script moves to add text labels indicating both the PDB ID and the render time in ns. A margin or border were added to each frame. The resultant 6,000 frames were 1080 × 1080px bitmaps of 5 MB/frame. Next, corresponding frames for each of the six insets in the composite were combined to create a single bitmap. The resultant 1,000 frames were then programmatically converted to video utilizing ffmpeg (libx264, very slow, CRF 28). The videograph and its frames were not smoothed or down-sampled until a final step in its production.

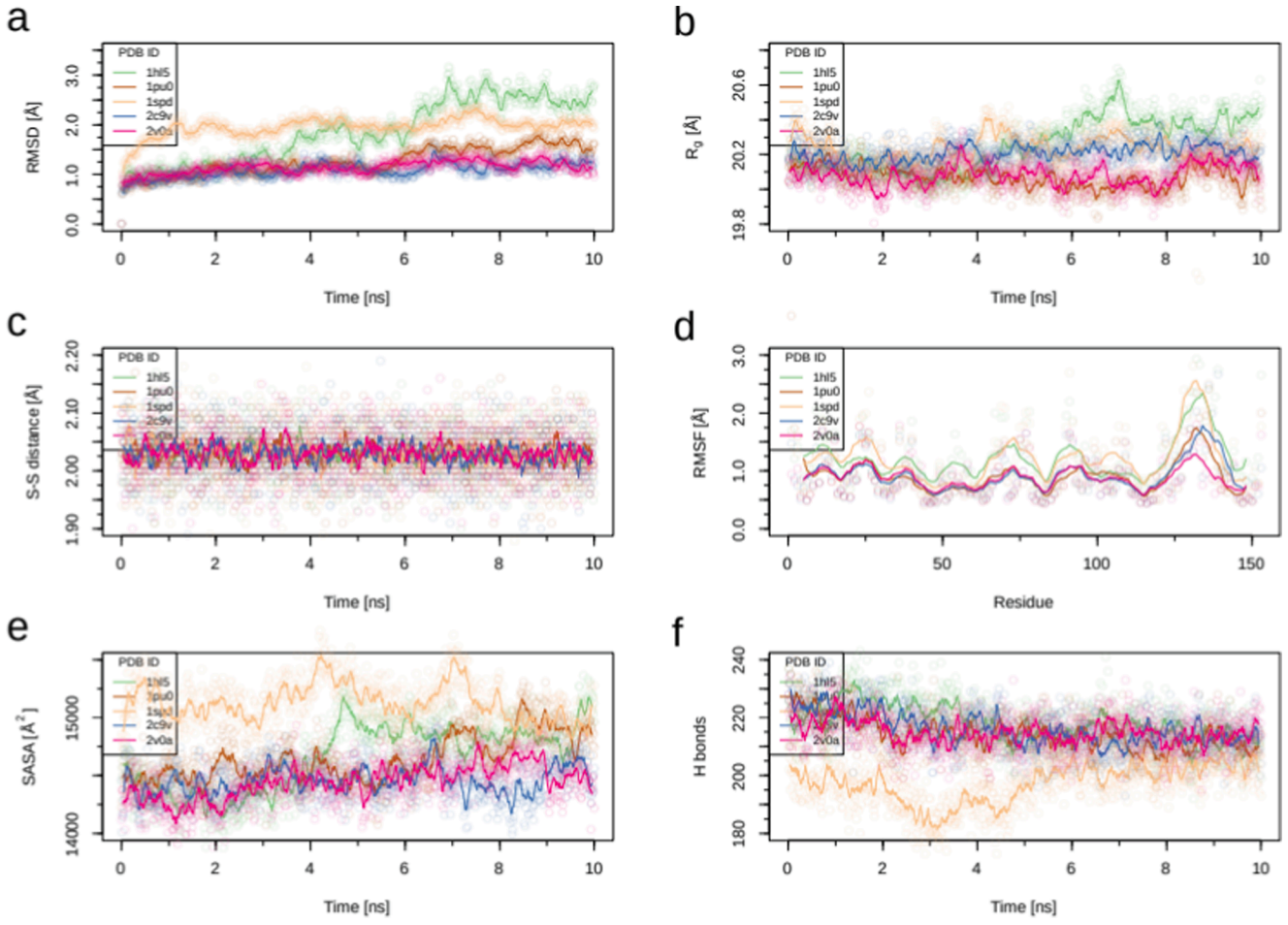

Fig. 1. MD on constructs from PDB IDS 1HL5, 1PU0, 1SPD, 2C9V, and 2V0A according to scale: (a) RMSD; (b) Radius of gyration; (c) First subunit distance of the intra-disulfide bond; (d) First subunit RMSF; (e) SASA; and (f) First subunit number of intramolecular hydrogen bonds. The S—S distance (c), RMSF (d), and H bonds (f) are shown for just one subunit of each dimer.

3. Results and discussion

3.1. Production MD simulations

Production MD simulations were computed at a rate of approximately 4 ns/hour for 10 ns of each MD simulation (0.01 ns resolution). The resultant analyses generated 1,000 data points for each dot plot of each panel in figures with the form of Fig. 1 which include Fig. S3 and Fig. S5. All data points were reported in every dot plot; for example, each of the six panels represent 5,000 unique data points for a total of 30,000 unique data points present in the vector format of the composite figure. Equilibrations and other data which match the production MD of Fig. 1 are given in Fig. S1 (Fig. 2).

Root mean square (RMS) displacement (RMSD) and RMS fluctuation (RMSF) data were collected in this study. RMS displacements and fluctuations are indicative of global conformational changes. Together with the PCA vectors, the RMSD and RMSF graphs enable qualitative interpretation of the MD simulation.

Radius of gyration (R_g) data were collected in this study. R_g is related to RMSD/RMSF through the root mean square distance. R_g represents the distance of various weighted system particles from its axis of rotation, and additionally describes the way in which mass is distributed over the axis of rotation of the biomolecule. R_g is also employed to study molecular multimerisation, and buckling and inversion.

Solvent-accessible surface area (SASA) data were collected in this study [84]. SASA represent the exterior solvation of the biomolecule to exclude its hydrophobic core, the core of which is a “cavity” intrinsic to most proteins [85]. A relative increase in SASA may indicate structural instabilities, solvent clashes, access to inner folds, and buried or ejected ions, whereas a drastic increase in SASA indicates that the structure is misfolded or denatured. Normal SASA fluctuations are characteristic of the solvated and ionized conditions of matrix.

The resolutions of the PDB crystallographs from which the constructs were derived were reported to PDB as: 1HL5 (1.80 Å); 1PU0 (1.70 Å), 1SPD (2.40 Å), 2C9V (1.07 Å), and 2V0A (1.15 Å). According to a comparison of the MD results from 1SPD relative to the MD results from 1PU0 and 1HL5, there is no clear correlation between the crystallographic resolution of a given PDB and the strength of its biophysical profile.

3.2. Comparative analyses

1HL5 and 1SPD have consistently elevated RMSD with RMSF values relative to the others, which are non-native WT hSOD1 dynamics that are more representative of large complexes that exhibit coarse molecular motions. The elevated RMSD of 1HL5 and 1SPD seen in Fig. 1a/d can indicate a major dysfunction such as protein misfolding, disordered regions, or conformational instability. The RMSD curve of 1HL5 is observed ramping up rather than leveling off or flattening, whereas the RMSD curve of 1SPD comparably flattens yet retains its elevation; these plot action show that 1HL5 is not adequately equilibrated to the MD simulation whereas 1SPD nonetheless is. The punctate steps in the 1HL5 plot action as observed past 3 ns, 5 ns, and 7 ns of MD simulation show the evolution of a reaction coordinate, transition state, conformational shift, or other concerted temporal change in structure.

Selection of a crystallographic template in a computational study is among the first and most crucial methodological decisions of the study. Two recent computational studies on SOD1 selected a PDB template without justifying that selection [19,86], which attenuated the potential breadth and impact of those results. Another recent computational study selected PDB ID 2C9V as its reference structure [87]; however, and despite its high atomic resolution, the popular usage of 2C9V is just poor precedent in the experimental design of chromatographic isolation of SOD1. The methods of the manuscript attached to 2C9V indicate that it is an experimental reconstitution construct [54]. 2C9V constructs exhibit non-native dynamics relative to other WT hSOD1. The artifacts imposed by the reconstitution of 2C9V such as in its chaotropic denaturation or metallic dialysis could explain the muddied molecular dynamics observed from 2C9V. The artifacts of reconstitution damage the dynamics of 2C9V to the extent of non-nativity. Other structures

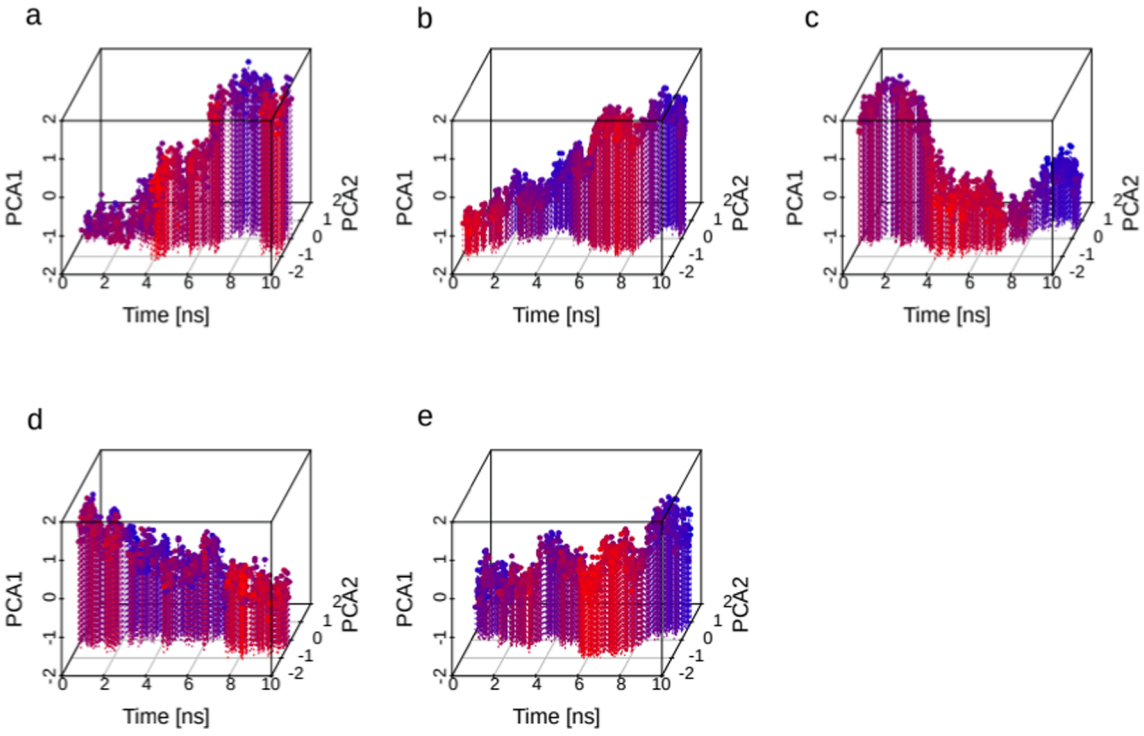

Fig. 2. Essential dynamics of eigenvectors 1 (PCA1) and 2 (PCA2) computed at the C-alpha position for the least squares fit and covariance analysis (PCA1 and PCA2, respectively) for each of PDB IDs (a) 1HL5, (b) 1PU0, (c) 1SPD, (d) 2C9V, and (e) 2V0A. The colorization of the data points and leading lines vary with the value of PCA2 as a spectrum from red to blue. (For interpretation of the references to colour in this figure legend, the reader is referred to the web version of this article.)

deposited by Strange *et al.* (2VOA, 1HL5) lack the experimental reconstitution and show appreciable native dynamics [51,55]. PDB ID 2C9U was also analysed by MD simulation in this work, but the construct exhibited deviant dynamics that likely resulted in a loss of its oxidized intra-disulfide bond over its first nanosecond of simulation.

3.3. Differential screening and selection

1PU0 was differentially selected as the ongoing reference structure. The many dimers of 1PU0 are defined as chains A/B, C/D, E/F, G/H, and I/J, each of which were assessed with 10 ns simulations. Dimer I/J of 1PU0 was selected as the reference structure in this study and for future work according to an analysis of its biophysical indicators relative to the biophysical indicators of comparative reference structure under identical conditions of simulation.

2V0A was not rejected at once due to its poor resolution (1.15 Å) alone but was also found highly resistant to dynamic perturbations. 2V0A thus has relatively limited use in potential experimental implementations. 2V0A was also found unfavorable across each of methodological design, signal-to-noise ratio, and interoperability concerns. 1SPD, 1HL5, and 2C9V exhibit non-native WT dynamics and deviant numerical values.

3.4. High-resolution molecular videography

A novel method of high-resolution molecular videography was developed to visualize MD simulations. Molecular videography is now an indispensable tool which enabled a fast qualitative determination of dynamics from what was the slow programmatic workflow of rendering and production.

The attached molecular videograph represented by Fig. 3 is paneled for each of six distinct MD simulations featuring 10 ns of simulation (60 ns total, 0.01 ns resolution). The videograph has a runtime of 20 s (540p/48 Hz resolution). The videograph were iteratively rendered from 6,000 total frames with 1,000 frames per panel of the composite figure. Identical videos were prepared at higher resolutions than that proctored here: 720p/60 Hz (73.3 MB) and 4 K/30 Hz (2.13 GB) (data not shown). The videograph attached to this manuscript has resolution 540p/48 Hz (53.2 MB), which is substantially reduced relative to the 4 K rendering, yet that still did not fail to resolve most particles in the animation. The attached videograph represented by Fig. 3 is a 53.2 MB deliverable derived from 196 GB of raw production content organized across 55 folders comprising 33E3 programmatically generated files. Inspection of the molecular videograph at once conveys major qualitative findings on its dynamics.

The concurrently displayed videos of each panel of the composite videograph represented by Fig. 3 were identically prepared and computed to simulation and visualisation, which enabled its comparative analysis across reference structures from PDB IDs: 1HL5, 1PU0, 1SPD, 2C9V, 2C9U, and 2V0A. In the attached videograph, the concurrent implementations and shared time axes have critically enabled its other temporal fluctuations, momentums, and trends; this reduction in system noise effectively amplified those temporal effects intrinsic to the PDB ID, whereas outside temporal effects were effectively silenced as just systemic constants. The preparation, computation, analysis, and graphical depiction of each of the video panels were programmatically prepared with identical treatments. That given the uniformity and large sample size (n = 6) of the composite videograph enable comparative analysis: the differences among panels within the composite can be solely and differentially attributed to intrinsic differences within the crystallographic templates.

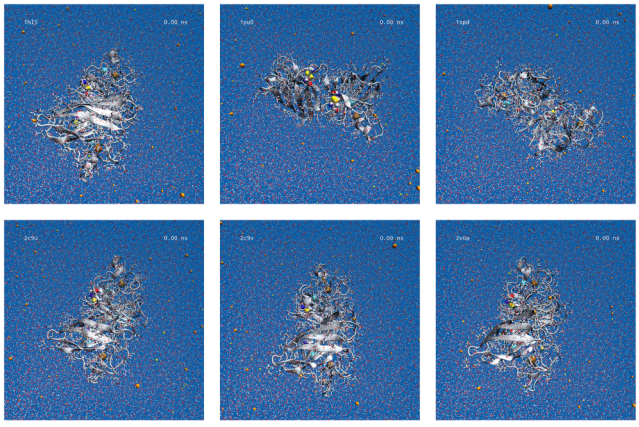

Fig. 3. Video of the defined MD simulations on constructs from PDB IDs 1HL5, 1PU0, 1SPD, 2C9V, and 2V0A. The composite of panels was solved up to 10 ns at a resolution of 0.01 ns, and a 20 s video was produced at 540p/48 Hz res.

1HL5, 1SPD, and 2C9U videographs exhibited erratic, non-native dynamics relative to the outstanding 1PU0, 2C9V, and 2V0A videographs, which indicate that the former lack metadynamic equilibration with the production matrix whereas the latter do not. The two-step equilibration method in early preparation of the videographs were consistently implemented without cause for concern. At approximately 5 ns in the 10 ns simulation on 2C9U, a cavity is seen to buckle and possibly even invert, which is a finding corroborated from the RMSD and R_g graphs for 2C9U (data not shown). The large rotational momentum and extreme beta-barrel flexibilities and fluctuations of 2V0A were absent in comparable simulation on 1PU0. In place, 1PU0 exhibited a centered, balanced, and oriented position for the duration of the videograph. The relatively exceptional molecular dynamics of 1PU0 were first recognized from its numerical values, which were later found corroborated via qualitative inspection of its molecular videograph.

3.5. Effect of ionic strength

Chains I/J of 1PU0 were assembled as constructs and subjected to varying ionic strength via [NaCl]. The ionic strength of the simulated matrix was adjusted by increasing [NaCl] from 0 mM to 1000 mM at points 0 mM, 100 mM, 200 mM, 300 mM, 400 mM, 500 mM, and 1000 mM, with potential energy, temperature, pressure, and density observed in Fig. 4. Fig. S5 gives the RMSD, radius of gyration, S—S distance, RMSF, SASA, and H bonding data, which show that increasing ionic strength uniformly increases RMSF and that 0 mM [NaCl] rendered the lowest SASA at most time points. An analysis of the essential dynamics of eigenvectors 1 and 2 (PCA1 and PCA2) are given in Fig. S6.

4. Conclusion

Superoxide dismutase 1 (SOD1) is a metalloenzyme that converts toxic superoxide to elemental dioxygen. Here, a panel of routinely implemented wildtype hSOD1 crystallographs were dynamically assayed in real-time by molecular dynamics (MD). Dozens of WT hSOD1 isoform crystalline constructs were observed for 10 ns at variable P, V, T, and ionic strength. RMS displacement and fluctuation, radius of gyration, SASA, hydrogen bond, and essential dynamic analyses were determined. Experiments specific to SOD1 biochemistry, viz. intra-disulfide and metallic bonding perturbations, were also observed. These results indicate that PDB ID 1PU0 should be selected as the reference structures for further computational studies on wild-type hSOD1.

The quantitative parameterizations and results of RMSD, RMSF, and PCA vectors as constrained to the MD simulation enabled a global qualitative view of the biomolecular dynamics. This novel method of molecular videography enabled the high-resolution videographic visualisation of dynamic simulation. The methods documented here are readily applied for similar computational efforts on other complex biomolecules.

These data are key for future approaches to SOD1 metadynamics, SOD1 folding and dimerization, its metallosulfidic isoforms, and

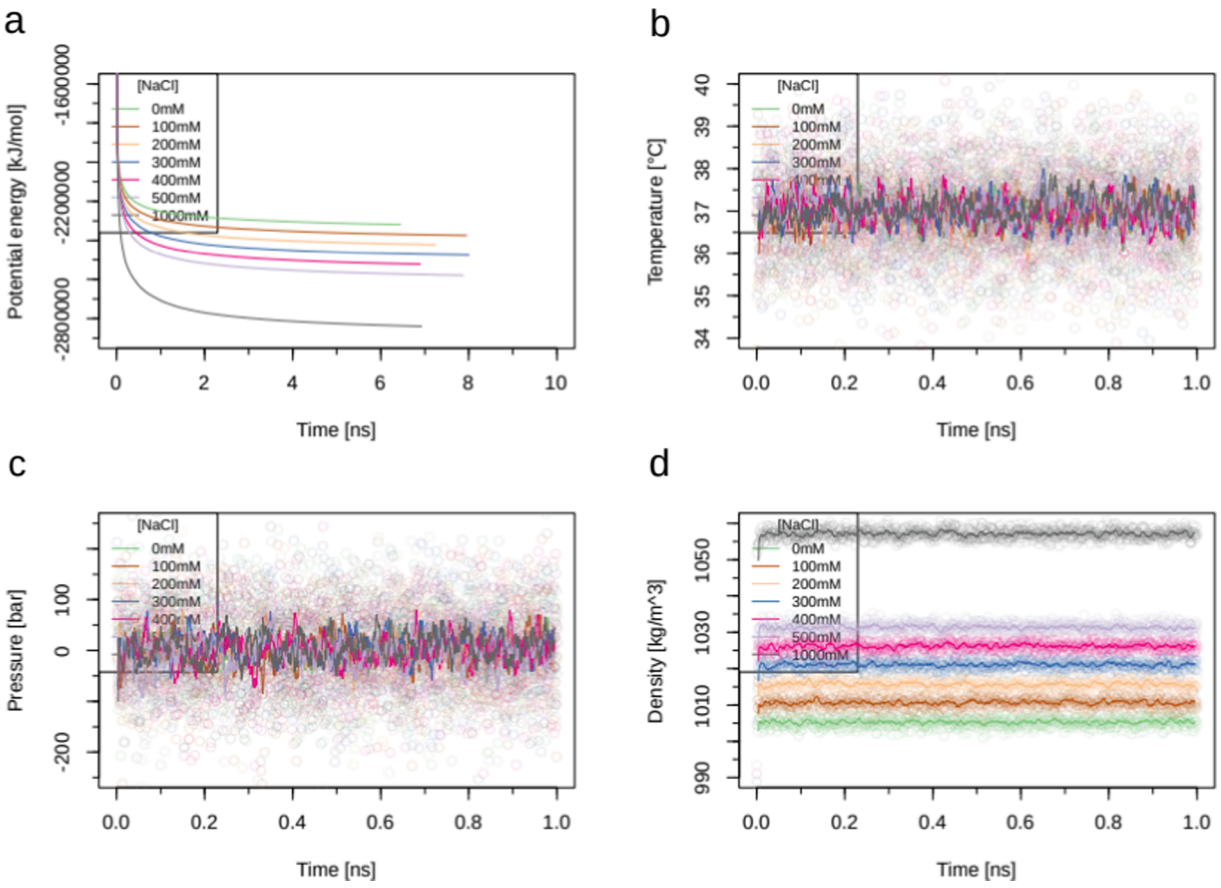

Fig. 4. Effect of increasing ionic strength on chains I/J of PDB ID 1PU0: (a) potential energy, (b) temperature, (c) pressure, and (d) density. The ionic strength of the simulated matrix was adjusted with [NaCl] from 0 mM to 1000 mM at points 0 mM, 100 mM, 200 mM, 300 mM, 400 mM, 500 mM, and 1000 mM, according to scale.

catalytic and mechanistic hypothesis-driven computational approaches on SOD1. Future MD analyses on SOD1 could include the metadynamics of a radicalized matrix, the complex modeling of SOD1 folding, dimerization, and subunit bonding, and other advanced delineations of the molecular configurations and reactive states of SOD1.

CRediT authorship contribution statement

Aron S. Workman: Conceptualization, Methodology, Software, Data curation, Visualization.

Declaration of Competing Interest

The authors declare that they have no known competing financial interests or personal relationships that could have appeared to influence the work reported in this paper.

Data availability

The authors are unable or have chosen not to specify which data has been used.

Appendix A. Supplementary material

Supplementary data to this article can be found online at https://doi.org/10.1016/j.comptc.2022.113929.

References

[1] T.W. Lyons, C.T. Reinhard, N.J. Planavsky, The rise of oxygen in Earth's early ocean and atmosphere, Nature 506 (7488) (2014) 307–315.
[2] S.S. Schatzman, V.C. Culotta, Chemical warfare at the microorganismal level: a closer look at the superoxide dismutase enzymes of pathogens, ACS Infect. Dis. 4 (2018) 893–903, https://doi.org/10.1021/ACSINFECDIS.8B00026/ASSET/IMAGES/ACSINFECDIS.8B00026.SOCIAL.JPEG_V03.
[3] A.W. Rutherford, A. Osyczka, F. Rappaport, Back-reactions, short-circuits, leaks and other energy wasteful reactions in biological electron transfer: redox tuning to survive life in O2, FEBS Lett. 586 (2012) 603–616, https://doi.org/10.1016/J.FEBSLET.2011.12.039.
[4] S.A. Hollingsworth, R.O. Dror, Molecular dynamics simulation for all, Neuron 99 (2018) 1129–1143, https://doi.org/10.1016/J.NEURON.2018.08.011.
[5] X. Liu, D. Shi, S. Zhou, H. Liu, H. Liu, X. Yao, Molecular dynamics simulations and novel drug discovery, Expert Opin. Drug Discovery 13 (1) (2018) 23–37.
[6] A. Ehn, J. Bood, Z. Li, E. Berrocal, M. Aldén, E. Kristensson, FRAME: femtosecond videography for atomic and molecular dynamics, Light Sci. Appl. 6 (9) (2017) e17045.
[7] K.R. Brorsen, N. Minezawa, F. Xu, T.L. Windus, M.S. Gordon, Fragment molecular orbital molecular dynamics with the fully analytic energy gradient, J. Chem. Theory Comput. 8 (2012) 5008–5012, https://doi.org/10.1021/CT3007869.
[8] R.A. Friesner, V. Guallar, Ab initio quantum chemical and mixed quantum mechanics/molecular mechanics (QM/MM) methods for studying enzymatic catalysis, Annu. Rev. Phys. Chem. 56 (1) (2005) 389–427.
[9] A.D. Mackerell, M. Feig, C.L. Brooks, Extending the treatment of backbone energetics in protein force fields: limitations of gas-phase quantum mechanics in reproducing protein conformational distributions in molecular dynamics simulations, J. Comput. Chem. 25 (11) (2004) 1400–1415.
[10] S. Tsuneyuki, T. Kobori, K. Akagi, K. Sodeyama, K. Terakura, H. Fukuyama, Molecular orbital calculation of biomolecules with fragment molecular orbitals, Chem. Phys. Lett. 476 (2009) 104–108, https://doi.org/10.1016/J.CPLETT.2009.05.069.
[11] F. Shimojo, S. Hattori, R.K. Kalia, M. Kunaseth, W. Mou, A. Nakano, K.I. Nomura, S. Ohmura, P. Rajak, K. Shimamura, P. Vashishta, A divide-conquer-recombine algorithmic paradigm for large spatiotemporal quantum molecular dynamics simulations, J. Chem. Phys. 140 (2014) 18A529, https://doi.org/10.1063/1.4869342.
[12] E. Srinivasan, R. Rajasekaran, Quantum chemical and molecular mechanics studies on the assessment of interactions between resveratrol and mutant SOD1 (G93A) protein, J. Comput. Aided Mol. Des. 32 (2018) 1347–1361, https://doi.org/10.1007/S10822-018-0175-1/FIGURES/10.
[13] E. Srinivasan, R. Rajasekaran, Molecular binding response of naringin and naringenin to H46R mutant SOD1 protein in combating protein aggregation using

density functional theory and discrete molecular dynamics, Prog. Biophys. Mol. Biol. 145 (2019) 40–51, https://doi.org/10.1016/j.pbiomolbio.2018.12.003.
[14] E. Srinivasan, R. Rajasekaran, Exploring the cause of aggregation and reduced Zn binding affinity by G85R mutation in SOD1 rendering amyotrophic lateral sclerosis, proteins: structure, Funct. Bioinform. 85 (2017) 1276–1286, https://doi.org/10.1002/PROT.25288.
[15] E. Srinivasan, R. Rajasekaran, Computational investigation of curcumin, a natural polyphenol that inhibits the destabilization and the aggregation of human SOD1 mutant (Ala4Val), RSC Adv. 6 (2016) 102744–102753, https://doi.org/10.1039/C6RA21927F.
[16] E. Srinivasan, R. Rajasekaran, Probing the inhibitory activity of epigallocatechin-gallate on toxic aggregates of mutant (L84F) SOD1 protein through geometry based sampling and steered molecular dynamics, J. Mol. Graph. Model. 74 (2017) 288–295, https://doi.org/10.1016/j.jmgm.2017.04.019.
[17] A. Sarkar, A.G. Gasic, M.S. Cheung, G. Morrison, Effects of protein crowders and charge on the folding of superoxide dismutase 1 variants: a computational study, J. Phys. Chem. B 126 (2022) 4458–4471, https://doi.org/10.1021/ACS.JPCB.2C00819.
[18] J. Zhu, J. Wang, W. Han, D. Xu, Neural relational inference to learn long-range allosteric interactions in proteins from molecular dynamics simulations, Nat. Commun. 13 (1) (2022) 1–16.
[19] A.C. Timucin, S.S. Cinaroglu, O.U. Sezerman, E. Timucin, Bridging the bridging imidazolate in the bimetallic center of the Cu/Zn SOD1 and ALS, Front. Chem. 9 (2021) 686, https://doi.org/10.3389/FCHEM.2021.716438/BIBTEX.
[20] P. Garg, S. Semmler, C. Baudouin, C. vande Velde, S.S. Plotkin, Misfolding-associated exposure of natively buried residues in mutant SOD1 facilitates binding to TRAF6, J. Mol. Biol. 434 (2022) 167697, doi: 10.1016/J.JMB.2022.167697.
[21] I. Jahan, S.M. Nayeem, Conformational dynamics of superoxide dismutase (SOD1) in osmolytes: a molecular dynamics simulation study, RSC Adv. 10 (2020) 27598–27614, https://doi.org/10.1039/D0RA02151B.
[22] E. Srinivasan, R. Rajasekaran, Computational investigation of the human SOD1 mutant, Cys146Arg, that directs familial amyotrophic lateral sclerosis, Mol. BioSyst. 13 (2017) 1495–1503, https://doi.org/10.1039/C7MB00106A.
[23] X. Li, Y. Zhong, C. Zhao, Trypsin binding with copper ions scavenges superoxide: Molecular dynamics-based mechanism investigation, Int. J. Environ. Res. Public Health 15 (1) (2018) 139.
[24] S.S. Mohseni, F. Nasri, K. Davari, S. Mirzaie, A. Moradzadegan, F. Abdi, F. Farzaneh, Identification of novel inhibitor against endonuclease subunit of Influenza pH1N1 polymerase: a combined molecular docking, molecular dynamics, MMPBSA, QMMM and ADME studies to combat influenza A viruses, Comput. Biol. Chem. 77 (2018) 279–290, https://doi.org/10.1016/j.compbiolchem.2018.08.005.
[25] P. Pongprayoon, How do the protonation states of E296 and D312 in OmpF and D299 and D315 in homologous OmpC affect protein structure and dynamics? Simulation studies, Comput. Biol. Chem. 53 (2014) 226–234, https://doi.org/10.1016/j.compbiolchem.2014.10.006.
[26] M. Karplus, J.A. McCammon, Molecular dynamics simulations of biomolecules, Nat. Struct. Biol. 9 (2002) 646–652, doi: 10.1038/nsb0902-646.
[27] J. Dvořák, M. Mańák, L. Váša, Predictive compression of molecular dynamics trajectories, J. Mol. Graph. Model. 96 (2020), https://doi.org/10.1016/j.jmgm.2020.107531.
[28] M. Miceli, S. Muscat, U. Morbiducci, M. Cavaglià, M.A. Deriu, Ultrasonic waves effect on S-shaped β-amyloids conformational dynamics by non-equilibrium molecular dynamics, J. Mol. Graph. Model. 96 (2020), https://doi.org/10.1016/j.jmgm.2019.107518.
[29] G. Muneeswaran, S. Kartheeswaran, M. Pandiaraj, K. Muthukumar, M. Sankaralingam, S. Arunachalam, Investigation of structural dynamics of Thrombocytopenia Cargeeg mutants of human apoptotic cytochrome c: a molecular dynamics simulation approach, Biophys. Chem. 230 (2017) 117–126, https://doi.org/10.1016/j.bpc.2017.09.004.
[30] X. Geng, J. Zhou, J. Guan, Side-chain dynamics analysis of KE07 series, Comput. Biol. Chem. 65 (2016) 148–153, https://doi.org/10.1016/j.compbiolchem.2016.09.007.
[31] H. Ogawa, M. Nakano, H. Watanabe, E.B. Starikov, S.M. Rothstein, S. Tanaka, Molecular dynamics simulation study on the structural stabilities of polyglutamine peptides, Comput. Biol. Chem. 32 (2008) 102–110, https://doi.org/10.1016/j.compbiolchem.2007.11.001.
[32] O.I. Omotuyi, H. Ueda, Molecular dynamics study-based mechanism of nefiracetam-induced NMDA receptor potentiation, Comput. Biol. Chem. 55 (2015) 14–22, https://doi.org/10.1016/j.compbiolchem.2015.01.004.
[33] P. Chairatana, J. Niramitranon, P. Pongprayoon, Dynamics of human defensin 5 (HD5) self-assembly in solution: molecular simulations/insights, Comput. Biol. Chem. 83 (2019), 107091, https://doi.org/10.1016/j.compbiolchem.2019.107091.
[34] Y.Y. Liu, X.Y. Feng, W.Q. Jia, Z. Jing, W.R. Xu, X.C. Cheng, Identification of novel PI3Kδ inhibitors by docking, ADMET prediction and molecular dynamics simulations, Comput. Biol. Chem. 78 (2019) 190–204, https://doi.org/10.1016/j.compbiolchem.2018.12.002.
[35] M.W. Hu, C.F. Hsu, B. Kim, The intrinsic dynamics of Cse1p and Xpot elucidated by coarse-grained models, Comput. Biol. Chem. 48 (2014) 45–54, https://doi.org/10.1016/j.compbiolchem.2013.11.003.
[36] M. Turner, S.T. Mutter, O.D. Kennedy-Britten, J.A. Platts, E.A. Permyakov, Molecular dynamics simulation of aluminium binding to amyloid-β and its effect on peptide structure, PLoS ONE 14 (6) (2019), e0217992, https://doi.org/10.1371/journal.pone.0217992.
[37] E.F. Healy, L. Cervantes, An in silico study of the effect of SOD1 electrostatic loop dynamics on amyloid–like filament formation, Eur. Biophys. J. 45 (2016) 853–859, https://doi.org/10.1007/s00249-016-1163-9.
[38] Z. Zuo, C. Gang, H. Zou, P.C. Mok, W. Zhu, K. Chen, H. Jiang, Why does β-secretase zymogen possess catalytic activity? Molecular modeling and molecular dynamics simulation studies, Comput. Biol. Chem. 31 (2007) 186–195, https://doi.org/10.1016/j.compbiolchem.2007.03.007.
[39] M. Turner, S.T. Mutter, J.A. Platts, Molecular dynamics simulation on the effect of transition metal binding to the N-terminal fragment of amyloid-β, J. Biomol. Struct. Dyn. 37 (2019) 4590–4600, https://doi.org/10.1080/07391102.2018.1555490.
[40] J.A. Platts, Quantum chemical molecular dynamics and metadynamics simulation of aluminium binding to amyloid-β and related peptides, R. Soc. Open Sci. 7 (2) (2020), https://doi.org/10.1098/rsos.191562.
[41] G. Muneeswaran, M. Pandiaraj, S. Kartheeswaran, M. Sankaralingam, K. Muthukumar, C. Karunakaran, Molecular dynamics simulation approach to explore atomistic molecular mechanism of peroxidase activity of apoptotic cytochrome c mutants, Inform. Med. Unlocked 11 (2018) 51–60, https://doi.org/10.1016/j.imu.2018.04.003.
[42] M. Singaravelu, A. Selvan, S. Anishetty, Molecular dynamics simulations of lectin domain of FimH and immunoinformatics for the design of potential vaccine candidates, Comput. Biol. Chem. 52 (2014) 18–24, https://doi.org/10.1016/j.compbiolchem.2014.08.002.
[43] M. Gupta, R. Chauhan, Y. Prasad, G. Wadhwa, C.K. Jain, Protein-protein interaction and molecular dynamics analysis for identification of novel inhibitors in Burkholderia cepacia GG4, Comput. Biol. Chem. 65 (2016) 80–90, https://doi.org/10.1016/j.compbiolchem.2016.10.003.
[44] R.H. Ghasemi, M. Keramati, M.H.S. Mojarrad, The effect of structure on improvement of the PNA Young modulus: a study of steered molecular dynamics, Comput. Biol. Chem. 83 (2019) 107133, https://doi.org/10.1016/j.compbiolchem.2019.107133.
[45] S.P. Singh, D.K. Gupta, Dynamic conformational ensembles regulate casein kinase-1 isoforms: insights from molecular dynamics and molecular docking studies, Comput. Biol. Chem. 61 (2016) 39–46, https://doi.org/10.1016/j.compbiolchem.2015.11.005.
[46] K.R. Raghi, D.R. Sherin, M.J. Saumya, P.S. Arun, V.N. Sobha, T.K. Manojkumar, Computational study of molecular electrostatic potential, docking and dynamics simulations of gallic acid derivatives as ABL inhibitors, Comput. Biol. Chem. 74 (2018) 239–246, https://doi.org/10.1016/j.compbiolchem.2018.04.001.
[47] A.N.R. da Silva, G.R.C. Pereira, L.G.A. Moreira, C.F. Rocha, J.F. de Mesquita, SOD1 in amyotrophic lateral sclerosis development – in silico analysis and molecular dynamics of A4F and A4V variants, J. Cell. Biochem. 120 (2019) 17822–17830, https://doi.org/10.1002/jcb.29048.
[48] C. Gueto-Tettay, J. Zuchniarz, Y. Fortich-Seca, L.R. Gueto-Tettay, J.C. Drosos-Ramirez, A molecular dynamics study of the BACE1 conformational change from Apo to closed form induced by hydroxyethylamine derived compounds, J. Mol. Graph. Model. 70 (2016) 181–195, https://doi.org/10.1016/j.jmgm.2016.10.006.
[49] M.L. Zhao, W. Wang, H. Nie, S.S. Cao, L.F. Du, In silico structure prediction and inhibition mechanism studies of AtHDA14 as revealed by homology modeling, docking, molecular dynamics simulation, Comput. Biol. Chem. 75 (2018) 120–130, https://doi.org/10.1016/j.compbiolchem.2018.05.006.
[50] E. Srinivasan, R. Rajasekaran, Computational simulation analysis on human SOD1 mutant (H80R) exposes the structural destabilization and the deviation of Zn binding that directs familial amyotrophic lateral sclerosis, J. Biomol. Struct. Dyn. 35 (2017) 2645–2653, https://doi.org/10.1080/07391102.2016.1227723.
[51] R.W. Strange, S. Antonyuk, M.A. Hough, P.A. Doucette, J.A. Rodriguez, P.J. Hart, L.J. Hayward, J.S. Valentine, S.S. Hasnain, The structure of holo and metal-deficient wild-type human Cu, Zn superoxide dismutase and its relevance to familial amyotrophic lateral sclerosis, J. Mol. Biol. 328 (2003) 877–891, https://doi.org/10.1016/S0022-2836(03)00355-3.
[52] M. DiDonato, L. Craig, M.E. Huff, M.M. Thayer, R.M.F. Cardoso, C.J. Kassmann, T. P. Lo, C.K. Bruns, E.T. Powers, J.W. Kelly, E.D. Getzoff, J.A. Tainer, ALS mutants of human superoxide dismutase form fibrous aggregates via framework destabilization, J. Mol. Biol. 332 (2003) 601–615, https://doi.org/10.1016/S0022-2836(03)00889-1.
[53] H.X. Deng, A. Hentati, J.A. Tainer, Z. Iqbal, A. Cayabyab, W.Y. Hung, E.D. Getzoff, P. Hu, B. Herzfeldt, R.P. Roos, C. Warner, G. Deng, E. Soriano, C. Smyth, H. E. Parge, A. Ahmed, A.D. Roses, R.A. Hallewell, M.A. Pericak-Vance, T. Siddique, Amyotrophic lateral ssclerosis and structural defects in Cu, Zn superoxide dismutase, Science 261 (1993) (1979) 1047–1051, https://doi.org/10.1126/SCIENCE.8351519.
[54] R.W. Strange, S.V. Antonyuk, M.A. Hough, P.A. Doucette, J.S. Valentine, S. S. Hasnain, Variable metallation of human superoxide dismutase: atomic resolution crystal structures of Cu–Zn, Zn–Zn and As-isolated wild-type enzymes, J. Mol. Biol. 356 (5) (2006) 1152–1162.
[55] R.W. Strange, C.W. Yong, W. Smith, S.S. Hasnain, Molecular dynamics using atomic-resolution structure reveal structural fluctuations that may lead to polymerization of human Cu-Zn superoxide dismutase, Proc. Natl. Acad. Sci. U.S.A. 104 (2007) 10040–10044, https://doi.org/10.1073/PNAS.0703857104.
[56] M.J. Abraham, T. Murtola, R. Schulz, S. Páll, J.C. Smith, B. Hess, E. Lindah, GROMACS: High performance molecular simulations through multi-level parallelism from laptops to supercomputers, SoftwareX 1–2 (2015) 19–25, https://doi.org/10.1016/J.SOFTX.2015.06.001.
[57] S. Páll, M.J. Abraham, C. Kutzner, B. Hess, E. Lindahl, Tackling exascale software challenges in molecular dynamics simulations with GROMACS, Lect. Notes Comput. Sci. (Includ. Subser. Lect. Notes Artif. Intell. Lect. Notes Bioinform.) 8759 (2014) 3–27, https://doi.org/10.1007/978-3-319-15976-8_1.

[58] S. Pronk, S. Páll, R. Schulz, P. Larsson, P. Bjelkmar, R. Apostolov, M.R. Shirts, J. C. Smith, P.M. Kasson, D. van der Spoel, B. Hess, E. Lindahl, GROMACS 4.5: a high-throughput and highly parallel open source molecular simulation toolkit, Bioinformatics 29 (2013) 845–854, https://doi.org/10.1093/BIOINFORMATICS/BTT055.
[59] B. Hess, C. Kutzner, D. van der Spoel, E. Lindahl, GROMACS 4: algorithms for highly efficient, load-balanced, and scalable molecular simulation, J. Chem. Theory Comput. 4 (2008) 435–447, https://doi.org/10.1021/CT700301Q.
[60] D. van der Spoel, E. Lindahl, B. Hess, G. Groenhof, A.E. Mark, H.J.C. Berendsen, GROMACS: fast, flexible, and free, J. Comput. Chem. 26 (2005) 1701–1718, https://doi.org/10.1002/JCC.20291.
[61] E. Lindahl, B. Hess, D. van der Spoel, GROMACS 3.0: a package for molecular simulation and trajectory analysis, Mol. Model. Ann. 7 (8) (2001) 306–317.
[62] H.J.C. Berendsen, D. van der Spoel, R. van Drunen, GROMACS: a message-passing parallel molecular dynamics implementation, Comput. Phys. Commun. 91 (1995) 43–56, https://doi.org/10.1016/0010-4655(95)00042-E.
[63] F. Eisenhaber, P. Lijnzaad, P. Argos, C. Sander, M. Scharf, The double cubic lattice method: efficient approaches to numerical integration of surface area and volume and to dot surface contouring of molecular assemblies, J. Comput. Chem. 16 (1995) 273–284, https://doi.org/10.1002/JCC.540160303.
[64] A. Bondi, van der Waals Volumes, Radii, J. Phys. Chem. 68 (1964) 441–451.
[65] R.H. Stote, M. Karplus, Zinc binding in proteins and solution: a simple but accurate nonbonded representation, Proteins: Struct. Funct. Bioinform. 23 (1995) 12–31, https://doi.org/10.1002/PROT.340230104.
[66] S. Obst, R.H. Stote, Comment on molecular dynamics simulations of zinc ions in water using CHARMM, J. Mol. Model. 4 (1998) 145, https://doi.org/10.1007/S008940050127.
[67] B.R. Brooks, R.E. Bruccoleri, B.D. Olafson, D.J. States, S. Swaminathan, M. Karplus, CHARMM: a program for macromolecular energy, minimization, and dynamics calculations, J. Comput. Chem. 4 (1983) 187–217, https://doi.org/10.1002/JCC.540040211.
[68] E. Lindahl, P. Bjelkmar, P. Larsson, M.A. Cuendet, B. Hess, Implementation of the CHARMM force field in GROMACS: analysis of protein stability effects from correction maps, virtual interaction sites, and water models, J. Chem. Theory Comput. 6 (2010) 459–466, https://doi.org/10.1021/CT900549R.
[69] J. Huang, S. Rauscher, G. Nawrocki, T. Ran, M. Feig, B.L. de Groot, H. Grubmüller, A.D. MacKerell, CHARMM36m: an improved force field for folded and intrinsically disordered proteins, Nat. Methods 14 (1) (2017) 71–73.
[70] W. Humphrey, A. Dalke, K. Schulten, VMD: visual molecular dynamics, J. Mol. Graph. 14 (1996) 33–38, https://doi.org/10.1016/0263-7855(96)00018-5.
[71] M. Valiev, E.J. Bylaska, N. Govind, K. Kowalski, T.P. Straatsma, H.J.J. van Dam, D. Wang, J. Nieplocha, E. Apra, T.L. Windus, W.A. de Jong, NWChem: a comprehensive and scalable open-source solution for large scale molecular simulations, Comput. Phys. Commun. 181 (2010) 1477–1489, https://doi.org/10.1016/J.CPC.2010.04.018.
[72] A.D. Becke, A new mixing of Hartree-Fock and local density-functional theories, J. Chem. Phys. 98 (2) (1993) 1372–1377.
[73] M. Caricato, G.W. Trucks, M.J. Frisch, K.B. Wiberg, Electronic transition energies: a study of the performance of a large range of single reference density functional and wave function methods on valence and rydberg states compared to experiment, J. Chem. Theory Comput. 6 (2010) 370–383, https://doi.org/10.1021/CT9005129/SUPPL_FILE/CT9005129_SI_001.PDF.
[74] C. Lee, W. Yang, R.G. Parr, Development of the Colle-Salvetti correlation-energy formula into a functional of the electron density, Phys. Rev. B 37 (2) (1988) 785–789.
[75] T. Yanai, D.P. Tew, N.C. Handy, A new hybrid exchange–correlation functional using the Coulomb-attenuating method (CAM-B3LYP), Chem. Phys. Lett. 393 (2004) 51–57, https://doi.org/10.1016/J.CPLETT.2004.06.011.
[76] M.M. Francl, W.J. Pietro, W.J. Hehre, J.S. Binkley, M.S. Gordon, D.J. DeFrees, J. A. Pople, Self-consistent molecular orbital methods. XXIII. A polarization-type basis set for second-row elements, J. Chem. Phys. 77 (7) (1982) 3654–3665.
[77] A.D. McLean, G.S. Chandler, Contracted Gaussian basis sets for molecular calculations. I. Second row atoms, Z = 11–18, J. Chem. Phys. 72 (10) (1980) 5639–5648.
[78] S.P. Keerthana, P. Kolandaivel, Study of mutation and misfolding of Cu-Zn SOD1 protein, J. Biomol. Struct. Dyn. 33 (2015) 167–183, https://doi.org/10.1080/07391102.2013.865104/SUPPL_FILE/TBSD_A_865104_SM7261.DOC.
[79] P.W. Rose, A. Prlić, A. Altunkaya, C. Bi, A.R. Bradley, C.H. Christie, L. di Costanzo, J.M. Duarte, S. Dutta, Z. Feng, R.K. Green, D.S. Goodsell, B. Hudson, T. Kalro, R. Lowe, E. Peisach, C. Randle, A.S. Rose, C. Shao, Y.-P. Tao, Y. Valasatava, M. Voigt, J.D. Westbrook, J. Woo, H. Yang, J.Y. Young, C. Zardecki, H.M. Berman, S.K. Burley, The RCSB protein data bank: integrative view of protein, gene and 3D structural information, Nucleic Acids Res. 45 (2017) D271–D281, doi: 10.1093/NAR/GKW1000.
[80] U. Essmann, L. Perera, M.L. Berkowitz, T. Darden, H. Lee, L.G. Pedersen, A smooth particle mesh Ewald method, J. Chem. Phys. 103 (19) (1995) 8577–8593.
[81] B. Hess, H. Bekker, H.J.C. Berendsen, J.G.E.M. Fraaije, LINCS: a linear constraint solver for molecular simulations, J. Comput. Chem. 18 (1997) 14631472, https://doi.org/10.1002/(SICI)1096-987X(199709)18:12.
[82] S. Miyamoto, P.A. Kollman, Settle: an analytical version of the SHAKE and RATTLE algorithm for rigid water models, J. Comput. Chem. 13 (1992) 952–962, https://doi.org/10.1002/JCC.540130805.
[83] G. Bussi, D. Donadio, M. Parrinello, Canonical sampling through velocity rescaling, J. Chem. Phys. 126 (1) (2007) 014101.
[84] B. Lee, F.M. Richards, The interpretation of protein structures: estimation of static accessibility, J. Mol. Biol. 55 (3) (1971), 379-IN4.
[85] M.L. Connolly, IUCr, Analytical molecular surface calculation, Urn:Issn:0021-8898. 16 (1983) 548–558, doi: 10.1107/S0021889883010985.
[86] N.G.M. Wells, G.A. Tillinghast, A.L. O'Neil, C.A. Smith, Free energy calculations of ALS-causing SOD1 mutants reveal common perturbations to stability and dynamics along the maturation pathway, Protein Sci. 30 (2021) 1804–1817, https://doi.org/10.1002/PRO.4132.
[87] G.R.C. Pereira, B. de Azevedo Abrahim Vieira, J.F. de Mesquita, Comprehensive in silico analysis and molecular dynamics of the superoxide dismutase 1 (SOD1) variants related to amyotrophic lateral sclerosis, PLoS ONE 16 (2021) e0247841, doi: 10.1371/JOURNAL.PONE.0247841.